

Switching variability factors in compliance-free metal oxide RRAM

D. Veksler, G. Bersuker, A. W. Bushmaker
 MTD, The Aerospace Corporation
 Los Angeles CA
 dmitry.veksler@aero.org

P. R. Shrestha, K. P. Cheung, J. P. Campbell
 NDCD, National Institute of Standards and Technology
 Gaithersburg, MD

Abstract— Switching variability in polycrystalline compliance-free HfO₂-based 1R RRAM is evaluated employing ultra-fast low voltage pulse approach. Changes in filament conductivity are linked to the variations of energy consumed in a switching process. This study indicates that variability is reduced (suppressed) in more resistive filaments.

Index Terms-- Neuromorphic computing, RRAM.

I. INTRODUCTION

Mobile neuromorphic computing (NC) systems introduce specific requirements to RRAM cells to be used as microelectronic "synapses". Sufficiently high stability and low variability of the memory states for the reliable gradual memory update is required in analog applications to implement adaptive synaptic changes. Formation and switching of the conductive filament in the metal oxides involves an atomic-level rearrangement that is a stochastic process resulting in high device-to-device and cycling variability [1]. Such stochasticity can be expected to reduce when redox processes are limited by a tighter control over the duration of the forming/switching operations and the oxide region where they take place. In this respect, the ultra-short pulse technique [2], which corresponds to actual circuitry operation frequencies, is an enabling tool to evaluate RRAM characteristics under use conditions. In this study, we focus on identifying operational factors, which can affect switching variability in hafnia-based filamental RRAM devices.

II. MEASUREMENTS SETUP

RRAM devices are formed by crossbar 50x50 nm MIM capacitors fabricated with an ALD polycrystalline 5nm HfO₂ film, overlaying oxygen scavenging Ti layer and TiN electrodes. Figure 1 show a setup, which delivers sufficiently short voltage pulses limiting energy dissipation and related redox processes that determines resistance of the formed filament and removes the need for a current compliance control.

The energy dissipated in the RRAM cell during forming can be calculated as:

$$E = \int_{t_0}^{t_0+t_{pulse}} V(t)I(t)dt \quad (1)$$

This research was partially supported by The Aerospace Corporation Internal Research and Development Program.

where $V(t)$ is the voltage pulse, $I(t)$ is the current through the RRAM cell during the pulse. The distribution of the post-forming resistance values at a given pulse width (Fig. 2) is driven by the variation of these forming energies, Eq. (1), caused by device-to-device variability of initial (pre-forming) precursor conductive paths, rather than variability of the forming process itself. By tuning the pulse amplitude, state resistance can be gradually, via multiple pulses, changed to the desirable level, Fig. 3. Cyclic switching between two resistance states was performed by employing a feedback system allowing to stop and flip the polarity of the programming pulse when the desired conductance state of the memory cell is reached. While LRS shows tight distribution over switching cycles, the HRS fluctuates. However, the frequency and amplitudes of large HRS fluctuation remain limited (up to R_{max}) during continuous switching (Fig. 4). It implies that these fluctuations are not associated with permanent structural changes, and observed resistance variations reflect random reversible processes (their origin will be discussed elsewhere).

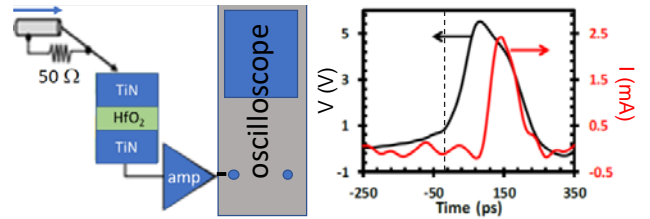


Figure 1. Short pulse RRAM switching setup. Example of measured voltage and current signal during RRAM forming extracted from oscilloscope measurements.

III. VARIABILITY AND ENERGY DISSIPATION

To understand the variability drivers, we compare cycle-to-cycle conductance variations, along with the corresponding distributions of switching energies. Due to extremely low parasitic capacitance in this crossbar architecture, it was possible to directly measure switching current down to ns pulses and extract switching energies, Eq. (1). In the samples that drift, device D - Fig. 5a, and in those that are stable, device S - Fig. 5b, switching characteristics (nominally identical devices D and S were formed targeting different post-forming

resistance. The more conductive device D exhibits higher cycling variability of both filament conductance (Fig. 5) and switching energy (Fig. 6).

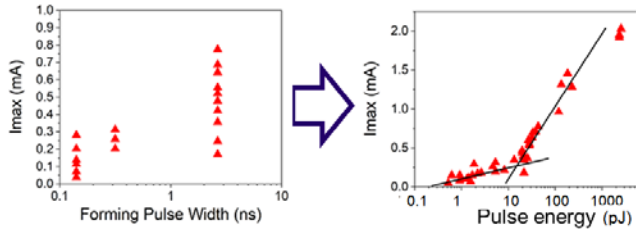


Figure 2. (a) Device-to-device distribution of the post-forming I_{max} vs. pulse durations. (b) I_{max} vs. energy consumed during forming pulse, E_{Form} . Above a certain critical energy value, the filament conductance increases at a much higher rate as indicated by the line slopes.

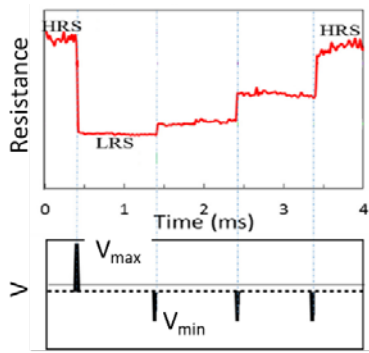


Figure 3. Resistance switching can be performed in analog regimes using multiple pulses ($|V_{max}|$ and $|V_{min}| < 1V$)

Since larger switching energy is consumed when the device is in a lower resistance state (higher current), variation in LRS conductance in the device D directly reflects on the variation of switching energy and, thus, they strongly correlate. The device with higher resistance, device S, demonstrates significantly tighter distributions of switching energies and conductance values in both HRS and LRS.

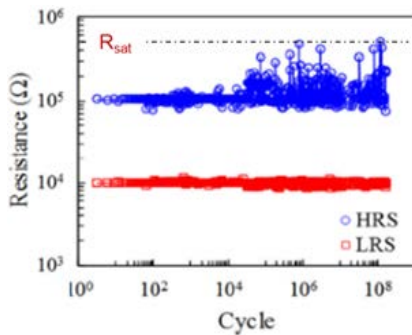


Figure 4. Endurance: LRS and HRS resistances vs. a number of switching cycles (in logscale). HRS resistance fluctuations are bounded, maximum variation of resistance, R_{sat} is observed approximately every 10000 cycles, fluctuations frequencies are constant throughout the entire switching cycle.

Conductivity values in 10^3 SET/ReSET cycles of the devices D and S are plotted vs. SET/ReSET energies

consumed in each of these cycles (calculated using Eq. 1) in Fig. 7. The same starting conductance states may lead to different conductivities after switching, as illustrated by an example of the ReSET switching data in Figs. 7,8. Higher starting LRS conductivities are associated with higher resulted HRS conductivities and switching energies (Fig. 8). It can be seen, however, that the variation of switching energy alone cannot account for the conductivity distribution at any given switching energy value. Indeed, the energy is determined by the contributions from both conductive states participating in interstate switching, when the voltage and duration of the switching pulses are hold constant, Eq. 1. In the ReSET process, LRS dominates: a current in this state determines the maximum consumed switching energies. In SET, a smaller portion of the overall switching time is associated with LRS, resulting in smaller SET energies in Fig. 7. Thus, the switching direction (SET or ReSET) also affects the outcome.

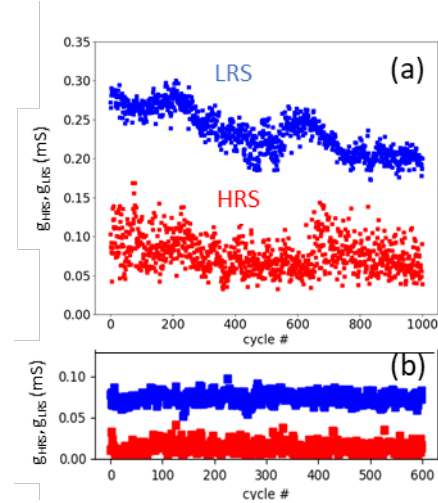


Figure 5. LRS and HRS conductance in (a) device D with drifting switching characteristics and (b) device S with stable switching characteristics.

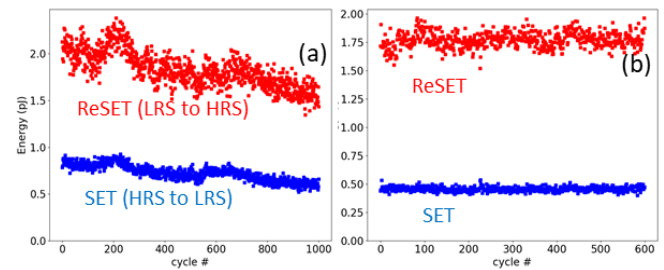


Figure 6. Energy consumed in each SET and ReSET switching event in (a) device D and (b) device S.

To identify the variability drivers, we start with the factors responsible for switching. Conductivity changes, that is differences between pre- and post- switching values: $\Delta g_{LRS} = g_{LRS} - g_{HRS}$ (SET) and $\Delta g_{HRS} = |g_{HRS} - g_{LRS}|$ (ReSET), are plotted vs. energies associated with the corresponding switching processes in Fig. 9. A much wider range of conductance

changes in device D can be linked not only to differences in switching energies, as expected in the case of varying resistance values (in Fig. 6), but also to the resistances of the starting states, from which the switching processes originate (large Δg spread-outs at each energy value).

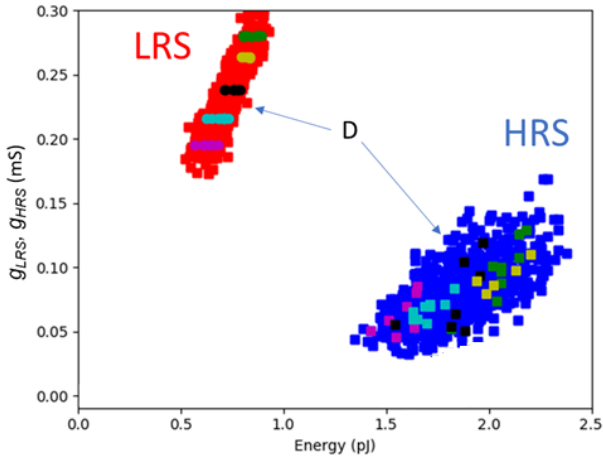


Figure 7. Cycle-to-cycle distributions of conductivity in LRS and HRS states vs. energy consumed in transitions (SET and ReSET, accordingly) to these states for the device D. Five groups of ReSET transitions (not consecutive) from different LRS are color-marked. After ReSETs the initially tight LRS distributions in each group transform into rather wide HRS distributions (marked by the same colors).

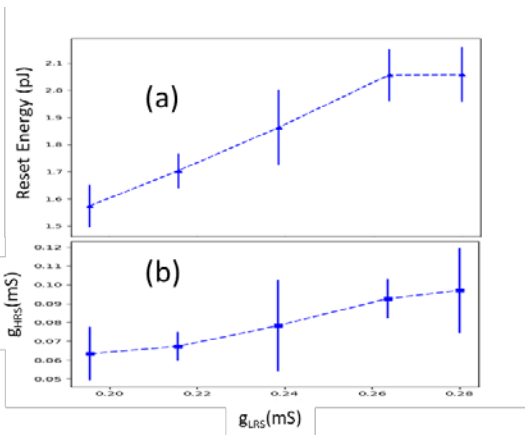


Figure 8. (a) Switching energy in the ReSET processes and (b) conductivity in HRS in switching cycles marked by colored symbols in Fig. 7. Bars show the standards deviation of measured data.

To outline the role of the starting state, Δg_{LRS} and Δg_{HRS} data of the device D in Fig. 7 are plotted vs. conductivity of the starting (pre-switching) states, from which each switching took place (Figs. 10, 12). In SET, consumed energy E_{Switch} is primarily determined by the final switching state since the LRS conductance dominates – therefore, larger starting resistance (larger g_{HRS}) should result in smaller Δg_{LRS} for a fixed E_{Switch} – in agreement with the data in Fig. 10. At the same time, Δg_{LRS} exhibits strong energy dependency as indicated by a larger slope of the energy gradient (normal to the equal-energy

regions marked by the parallel dart lines) in Fig. 10. The trends of resulted LRS conductance and switching energy E_{Switch} correlate, Fig. 11. In SET process, the effect of variation of conductance of starting state, g_{HRS} , is weaker than the effect of the switching energies, as seen in Δg_{LRS} dependency on the slope of the dart line in Fig. 10.

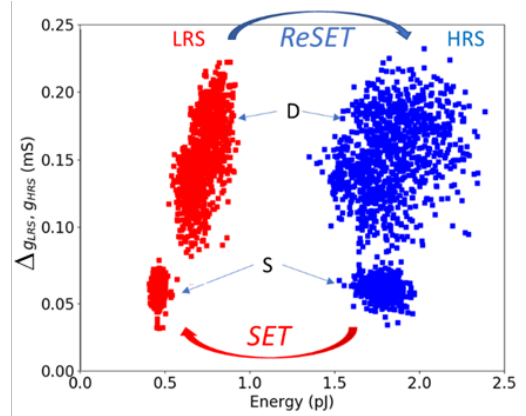


Figure 9. Distributions of the relative conductance changes, $\Delta g_{LRS} = g_{LRS} - g_{HRS}$ (SET) and $\Delta g_{HRS} = |g_{HRS} - g_{LRS}|$ (ReSET), vs. corresponding switching energies for each cycle in D and S devices. Y-axis corresponds to the conductancies resulted from SET and ReSET switching, while x-axis contains values of energies released during switching.

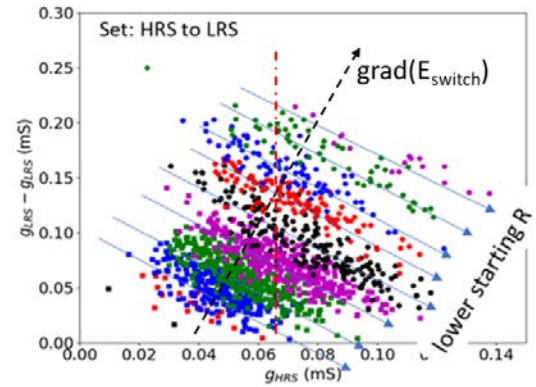


Figure 10. Conductivity changes in HRS to LRS switching (device D), Δg_{LRS} , vs. starting g_{HRS} values. Symbols of the same color and type (along each individual dart line) identify switching operations occurred with same energy.

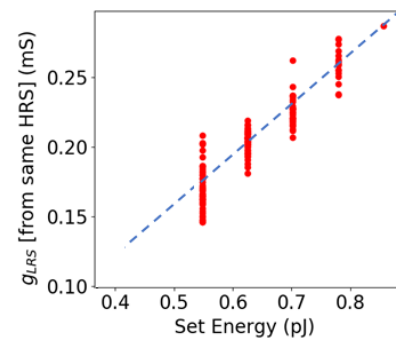


Figure 11. Post-switching LRS conductance vs. energy for switching from the same HRS state as marked by the vertical dash-dot line in Fig. 10.

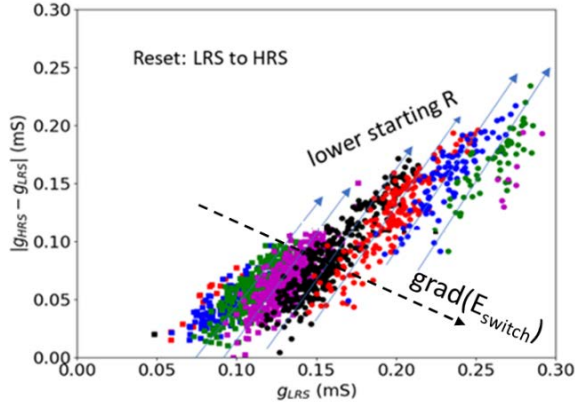


Figure 12. Conductivity changes in Reset switching, $\Delta g_{\text{HRS}} = |g_{\text{HRS}} - g_{\text{LRS}}|$ vs. starting LRS conductance values. Symbols of the same color (along each individual dashed line) identify switching operations occurred with same energy.

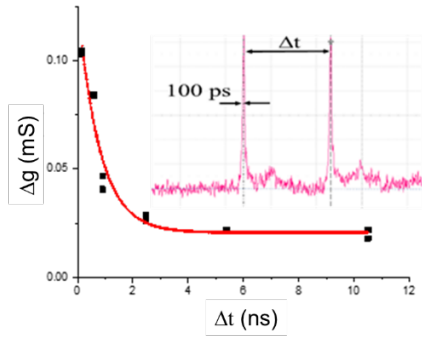


Figure 13. Correlated effect of repeated pulses. Relative increase of RRAM conductance, Δg_{HRS} vs. time delay, Δt , between 2 sequential set pulses (see inset) when $\Delta t \leq 2\text{ns}$.

In ReSET, an opposite trend is expected: since switching energy E_{Switch} is dominated by LRS, larger starting g_{LRS} should lead to larger Δg_{HRS} , as indeed is observed in Fig. 12. Thus, HRS resistance is primarily determined by the starting LRS value: consequently, lower starting resistance leads to greater switching window. The corresponding energy gradient is smaller than that of the starting resistances (as indicated by arrows in Fig. 12). In ReSET, resistance change is driven by the switching energy, which is controlled by LRS – higher g_{LRS} results in higher g_{HRS} . In SET, initially the beginning of the switching process, resistance change is driven by the consumed HRS energy, which then increases along with the increase of g_{LRS} , resulting in a weaker Set energy dependency/distribution, as seen in Fig. 7.

We speculate that LRS variability results in variations of the consumed energy (E_{Switch}) and temperature in the vicinity of the filament (depends on LRS current) during switching that strongly affects redox processes [4], and, in turn, may cause Reset cycling instability.

To assess the effect of temperature on switching, we studied how RRAM resistance is modulated by the timing between two sequential programming pulses (Fig. 13). Reducing the time

interval between pulses below 2 ns results in significant amplification of their effect on resistance. It's consistent with theoretical expectations that, by increasing local temperature around the conductive path [1], the first pulse magnifies the structural changes induced by the subsequent pulse. The filament resistance in hafnia-based RRAM can be gradually and linearly changed depending on polarity of programming pulse, Fig 14 (the corresponding switching energy was estimated to be in sub pJ range, Fig. 15), that is an essential feature of an artificial synapse.

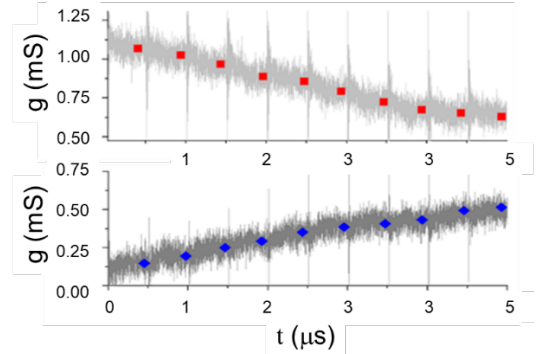


Figure 14. Semi-linear increase and decrease of the RRAM conductance under continuous SET (0.75 V) and RESET (1.25 V) pulses. Program pulse width is 100 ps. Square marks on the conductance traces correspond to averaged values of the RRAM conductance after each pulse.

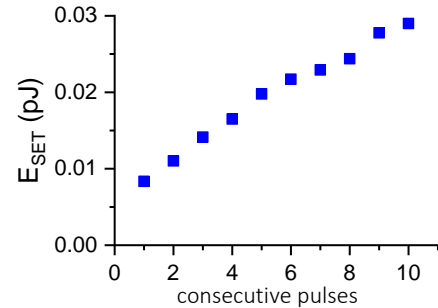


Figure 15. Upper limit estimate of the energy consumed in each SET pulse operation in Fig. 14.

IV. CONCLUSION

This study indicates that RRAM evaluation should be done under the frequencies and voltages conditions close to intended circuitry applications. In the sub-ns operation time range, hafnia-based devices demonstrate compliance-free forming and ultra-low energy switching.

Correlation between switching variability and energy consumed during switching process points to the effect of random structural changes in a certain (likely minor) region of the conductive filament. Higher filament resistance leads to lower dissipated energy: resulted lower temperature slows redox kinetic that is expected to suppress variability. Such property of hafnia-based devices facilitates their use in large scale neuromorphic cross-bar architectures.

References:

1. G. Bersuker, D. Gilmer, D. Veksler "Metal oxide resistive random-access memory (RRAM) technology" *Advances in Non-volatile Memory and Storage Technology*, Elsevier (2019).
2. P. R. Shrestha, D. Nminibapiel, J. H. Kim, J. P. Campbell, K. P. Cheung, S. Deora, G. Bersuker, and H. Baumgart, Energy control paradigm for compliance-free reliable operation of RRAM, in proc. 2014 IEEE International Reliability Physics Symposium, MY.10.1-MY.10.4 (2014)
3. D. M. Nminibapiel, D. Veksler, P. R. Shrestha, Ji-H. Kim, J. P. Campbell, J. T. Ryan, H. Baumgart, and K. P. Cheung, "Characteristics of Resistive Memory Read Fluctuations in Endurance Cycling," in *IEEE Electron Device Letters*, **38**, pp. 326-329 (2017).
4. G. Bersuker, D. Veksler, D. M. Nminibapiel, P. R. Shrestha, J. P. Campbell, J. T. Ryan, H. Baumgart, M. S. Mason, K. P. Cheung, *Journal of Comp. Electronics*, **16**, 1085-1094 (2017).